Available online at www.sciencedirect.com
ScienceDirect
International Journal of Heat and Mass Transfer 50 (2007) 2838–2854
International Journal of HEAT and MASS TRANSFER
www.elsevier.com/locate/ijhmt

Hydrodynamic cavitation and boiling in refrigerant (R-123) flow inside microchannels

Brandon Schneider, Ali Koşar, Yoav Peles *

Department of Mechanical, Aerospace and Nuclear Engineering, Rensselaer Polytechnic Institute, Troy, NY 12180, USA

Received 8 February 2006; received in revised form 1 November 2006
Available online 6 March 2007

Abstract

This research article investigates the effect that hydrodynamic cavitation has on heat transfer. The fluid medium is refrigerant R-123 flowing through 227 μm hydraulic diameter microchannels. The cavitation is instigated by the inlet orifice. Adiabatic tests were conducted to study the two-phase cavitating flow morphologies and hydrodynamic characteristics of the flow. Diabatic experiments were performed resulting in surface temperatures under heat fluxes up to 213 W/cm^2 and mass velocities from 622 kg/m^2 s to 1368 kg/m^2 s. Results were compared to non-cavitating flows at the same mass velocities. It was found that the cavitating flows can significantly enhance the heat transfer. The heat transfer coefficient of the cavitating flows was larger than the non-cavitating flows by as much as 84%. Single-phase and two-phase heat transfer coefficients have been elucidated and employed to deduce the heat transfer mechanism prevailing under boiling conditions with and without the presence of cavitation.

Keywords: Microchannels; Cavitation; Boiling; Orifice; MEMS

1. Introduction

Christopher Earls Brennen in his insightful *Cavitation and Bubble Dynamics* book [1] states that "A rough but useful way of distinguishing [cavitation and boiling] processes is to define cavitation as the process of nucleation in a liquid when the pressure falls below the vapor pressure, while boiling is the process of nucleation that occurs when the temperature is raised above the saturated vapor/liquid temperature". The engineering communities are in fact divided across this line, and researchers studying heat transfer seldom interact with their fellows investigating cavitation. Heat transfer is infrequently studied in the presence of cavitation, and the existing studies are mostly concerned with ultrasonic cavitation [2–9]. This is surprising since it is frequently argued that the formation of two-phase flow is commonly associated with significant heat transfer enhancement. The flow morphologies formed in cavitating flows (e.g., annular, bubbly, etc.) may significantly augment the thermal performance of heat exchangers. Presently, very limited data is available to validate/invalidate this hypothesis, and to provide engineering guidelines and scientific knowledge about this phenomenon.

Hydrodynamic cavitation has been extensively investigated in the last century [1,10–16] and is a rich field of current study. The present cavitation knowledge (experimental and analytical) has contributed immensely towards improving the design of rudimentary conventional scale fluid machinery like hydrofoils [17,18], valves [18–22], orifices [20–30] and venturis [31–40]. Mishra and Peles [41–45] in several recent publications have extended this research endeavor to study hydrodynamic cavitation in micro systems. Their results revealed unique cavitating flow morphologies which were not reported previously in cavitating macro scale systems, and have inspired Schneider et al. [46] to study heat transfer in the presence of cavitating de-ionized (DI) water flow in microchannels. Their study

* Corresponding author. Tel.: +1 518 276 2886; fax: +1 518 276 2623.
E-mail address: pelesy@rpi.edu (Y. Peles).

0017-9310/$ - see front matter © 2007 Elsevier Ltd. All rights reserved.
doi:10.1016/j.ijheatmasstransfer.2007.01.002

Nomenclature

A	area, m^2
A_f	total fin surface area, m^2
A_p	planform area (surface area of silicon block), m^2
A_s	surface area, m^2
A_t	total heat transfer area $(A_b + \eta_f A_f)$, m^2
c_p	specific heat, kJ kg^{-1} K
D_h	channel hydraulic diameter, m
f	friction factor
$F_{3,4}$	correction factor in Eq. (18)
G	mass flux, kg m^{-2} s^{-1}
h	heat transfer coefficient, W m^{-2} °C^{-1}
$\bar{h}_{sp}$	average single-phase heat transfer coefficient, W m^{-2} °C^{-1}
$\bar{h}_{tp}$	average two-phase heat transfer coefficient, W m^{-2} °C^{-1}
H	channel height, fin height, m
h_{fg}	heat of vaporization, kJ kg^{-1}
I	electrical current, A
k	isotropic constant Eq. (15)
k_{fluid}	thermal conductivity of the fluid, W m^{-1} °C^{-1}
k_s	thermal conductivity of the Silicon block, W m^{-1} °C^{-1}
L	channel length, m
L_{sp}	length single phase, m
L_{th}	thermal entrance length, m
L_{tp}	length two-phase, m
MAE	mean absolute error
m	fin parameter in Eq. (8)
$\dot{m}$	mass flow rate, kg s^{-1}
N	number of microchannels
Nu	Nusselt number
$\overline{Nu}$	average Nusselt number
P	electrical power, W
P_{GO}	partial pressure of oxygen, kPa
p_e	exit pressure, kPa
p_i	inlet pressure, kPa
P_{oe}	pressure in orifice, kPa
p_v	vapor pressure, kPa
Pr	Prandtl number
q''	heat flux, W cm^{-2}
$\dot{Q}_{loss}$	heat loss, W
R	electrical resistance, Ω
R_0	initial radius of vapor bubble, m
R_f	finial radius of vapor bubble, m
Re	Reynolds number based on the channel hydraulic diameter
S	surface tension, N m^{-1}
t	time, s
t_s	thickness of silicon block, m
T	temperature, °C
$\overline{T}$	average surface temperature, °C
T_e	exit temperature, °C
$\overline{T}_F$	average fluid temperature, °C
$\overline{T}_{heater}$	average heater surface temperature, °C
T_i	inlet temperature, °C
u	liquid velocity at the inlet restrictor, m s^{-1}
V	electrical voltage, V
W	channel width, m
W_b	distance between two microchannels, m
x	quality
z	distance from the inlet, m

Greek symbols

β	aspect ratio
Δp	pressure drop, kPa
ΔT_i	temperature difference between $\overline{T}$ and T_i, °C
η_f	fin efficiency
η_o	overall fin efficiency
ρ	density, kg m^{-3}
σ	cavitation index

Subscripts

amb	ambient
e	exit
F	fluid
f	fin
i	inlet
m	mean
s	surface
sp	single phase
tp	two phase

has revealed significant heat transfer enhancement when cavitation was instigated.

Like cavitation, heat transfer is a well defined and established field of study. In recent years the heat transfer community has been closely examining a new class of thermal devices termed by Thome [47] micro-thermal-mechanical systems (MTMS). Single-phase/boiling flow in microchannels [47–71]/pin fin heat sinks [72–75], along with various other configurations have been studied. A primary motive in this new effort is to provide the electronics industry with cooling solutions that will enable the development of exceedingly high power dissipation electronics like CPUs, and laser diodes. The results presented by Schneider et al. [46] on hydrodynamic cavitation enhanced heat transfer offer a promising avenue to pursue as part of this exciting effort. However, much is still unknown about the effect of cavitation on heat transfer.

This study is aimed at extending the current scientific knowledge of this phenomenon by presenting results of cavitating flow of R-123 in a microchannel device established by inlet orifices. Heat transfer coefficients during cavitating conditions have been obtained and compared

to the corresponding values of non-cavitating flow. As a result, multifarious cavitating flow morphologies have been identified under various hydraulic conditions. The results clearly indicate the potential merit of hydrodynamic cavitation as a phenomenon which can be exploited to enhance heat transfer. A brief review on cavitating flow through orifices is provided in Section 2. The design and fabrication of the micro-orifice are presented in Section 3, while the experimental setup description and the experimental procedure are provided in Section 4. Section 5 is devoted to the discussion of the experimental results and Section 6 presents the conclusions of this investigation.

2. Background

Fluid flow through orifices is characterized by a significant drop in the static pressure right after the orifice. The hydraulic grade lines (HGL) for flow through an orifice are shown in Fig. 1. A sharp pressure drop is observed downstream of the micro-orifice because of the sudden reduction in the flow area. The reduction in static pressure is accompanied by an acceleration of the fluid and a subsequent increase in the fluid velocity between points 1 and 2. The location (point 2) where the static pressure drops to its minimum and the velocity rises to its maximum, is termed the *Vena Contracta*. Therefore, large dynamic heads are present at the orifice throat (*Vena Contracta*) and can cause the static pressure to fall to a very low value.

The rudimentary requirement for the formation of hydrodynamic cavitation is the reduction of static pressure to a critical value. This can be achieved by dramatically changing the area of a microchannel by introducing a micro-orifice in the flow field. A variety of cavitating and non-cavitating flow regimes are encountered as the exit pressure is brought down. A reduction in the exit pressure is accompanied by a reduction in the static pressure at the *Vena Contracta* (HGL 1). Proceeding on similar lines and further reducing the exit pressure causes the static pressure at the *Vena Contracta* to fall and results in an increase in the discharge (HGL 2). When the *Vena Contracta* pressure reaches a critical value, it promotes the growth of nuclei (submicron bubbles) by diffusion of dissolved gas into the available nuclei. The static pressure is still above the vapor pressure of the liquid therefore the mechanism of bubble growth is dominated by gaseous cavitation. Further reduction of the exit pressure lowers the static pressure at the *Vena Contracta* to the vapor pressure of the liquid (HGL 3) and forms a vapor cavity. After this physical limit has been reached, further attempts to increase the flow rate by reducing the exit pressure are ineffective. This is defined as choked flow or choked cavitation. The exit pressure loses its control over the discharge.

3. Device overview and fabrication

Fig. 2a displays the microchannel device consisting of five 1-cm long, 200-μm wide and 264-μm deep, parallel microchannels, spaced 200 μm apart. In order to minimize ambient heat losses an air gap was formed along the two ends of the side walls, and inlet and exit plenums were

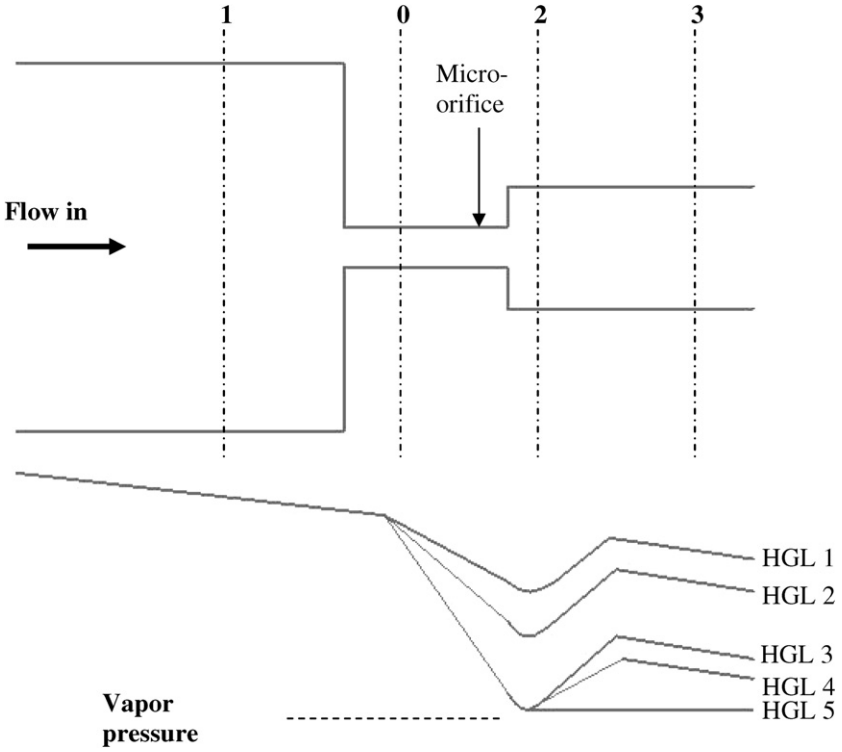

Fig. 1. Hydraulic gradient line (HGL) for fluid flow through a micro-orifice.

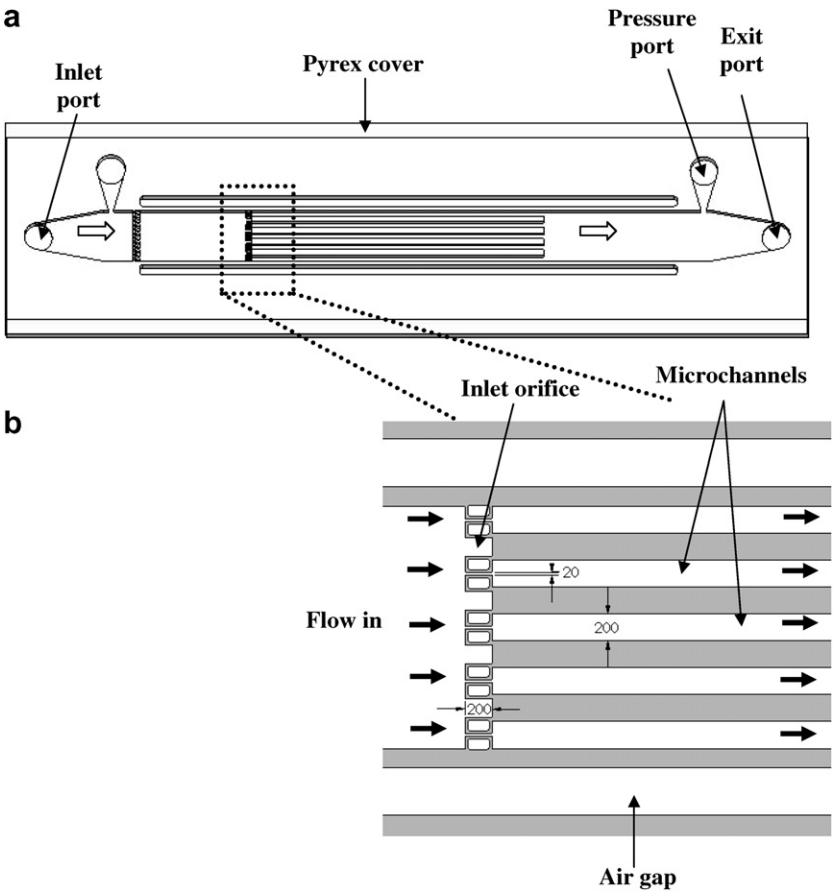

Fig. 2. (a) CAD model of the microchannel device and (b) geometry of the inlet region (dimensions in μm).

etched into the thin silicon substrate (~150 μm). A heater was deposited on the backside to deliver the heating power and serves as a thermistor for temperature measurements. A Pyrex substrate was used to seal the device from the top and allow flow visualization. Flow distributive pillars were used to provide homogeneous distribution of flow in the inlet. They are arranged in two columns of 12 circular pillars having diameters of 100 μm. The transverse pitch between the pillars is 150 μm and equal to the longitudinal pitch. Five 20-μm wide, 200-μm long orifices were installed (Fig. 2b) at the entrance of each channel to promote cavitation events.

4. Experimental test rig and procedure

4.1. Microchannel fabrication method

The MEMS (MicroElectroMechanical Systems) device was micromachined on a polished double-sided n-type ⟨100⟩ single crystal silicon wafer employing techniques adapted from IC manufacturing. The device was equipped with pressure ports at the inlet and at the exit to obtain accurate static pressures measurements. The microfabrication processes used to fabricate the device are identical to the processes detailed in several previous papers [46,56] and therefore not comprehensively discussed here.

4.2. Experimental test rig

A schematic of the experimental setup is shown in Fig. 3. Major components are a pump, a filter, flow meters (rotameters), a packaging module, and a microchannel device. The microchannel device is packaged by sandwiching it between two plates. The fluidic seals are forged using miniature "o-rings". The external electrical connections to the heater are installed from beneath through spring-loaded pins, which connect the heater to electrical pads residing away from the main MEMS device body. Resistance, pressure, and flow measurements are taken at a fixed flow rate in the loop. The electrical power is supplied to the device with an INSTEK programmable power supply, while electrical current and voltage are measured through an accurate HP digital multimeter. A HNP Mikrosysteme micro annular gear pump capable of generating flow rates from 0.3 ml/min to 18 ml/min is used to propel the liquid from a reservoir through the MEMS device. Inlet and exit pressures are measured via pressure transducers. An Omega F-111 flow meter is used for flow rate measurement. Pressure and flow rate data are acquired together with the voltage and current data and are sent to the spreadsheet file for data reduction. The flow is proctored with a microscope and flow images are taken via a Vision Research Phantom V-4 series high-speed camera capable of capturing frames with a rate

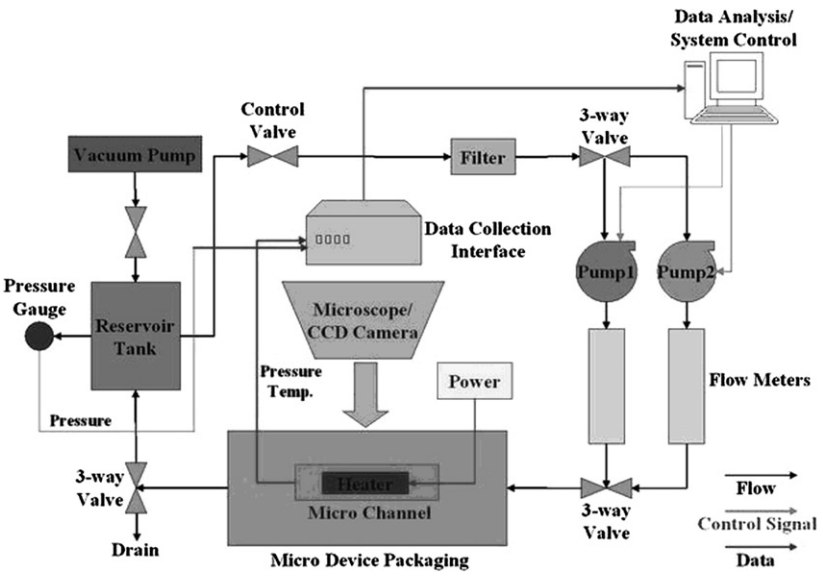

Fig. 3. Experimental setup.

of up to 90,000 frames/s, with a maximum resolution of 512×512 pixels, and a minimum exposure time of 2 μs.

4.3. Experimental procedures and data reduction

In this study adiabatic and diabatic conditions were tested in the presence of cavitating and non-cavitating flows. The diabatic experiments were performed for conditions corresponding to exit mass qualities smaller and larger than zero. Refrigerant R-123 was used as the working fluid at three fixed flow rates. For the cavitating flow conditions, the exit pressure was reduced until the desired cavitating conditions were reached. For the non-cavitating flow conditions, the inlet and exit pressures were carefully controlled to maintain the proper flow rate while keeping the flow from cavitating. Prior to recording data the device was calibrated in a well insulated and temperature controlled oven, and a heater electrical resistance–temperature linear calibration curve was generated (Fig. 4). A standard deviation of 0.16 °C was obtained between the individual data points and the calibration curve. The curve was then used during data reduction to extract the average temperature of the device. Thereafter, voltage was applied in 0.5 V increments to the heater, and the current/voltage data were recorded along with pressure data from the inlet and exit pressure ports once steady state was reached. The power to the device was turned off when the average surface temperature of the heater rapidly increased with minor increase in the input power, indicating critical heat flux (CHF) conditions. Flow visualization through the high-speed camera and microscope complemented the measured data and enabled the characterization of flow patterns prevailing along the microchannels. Images of flow patterns were recorded at both adiabatic and diabatic tests for each operating condition.

The dissolved gas concentration in the liquid is an important parameter in cavitation and boiling experiments [76,77]. However, measuring dissolved gas content in non-aqueous solutions (e.g., refrigerants) is a very arduous task and is an issue that has not been fully resolved by the scientific community. To overcome this matter, it is common to report the saturation pressure to which the liquid was exposed before experimentation. In the current study the dissolved gas concentration of the refrigerant corresponds to the saturation conditions at atmospheric pressure and room temperature.

Data obtained from the voltage, current and pressure measurements was used to calculate the cavitation index,

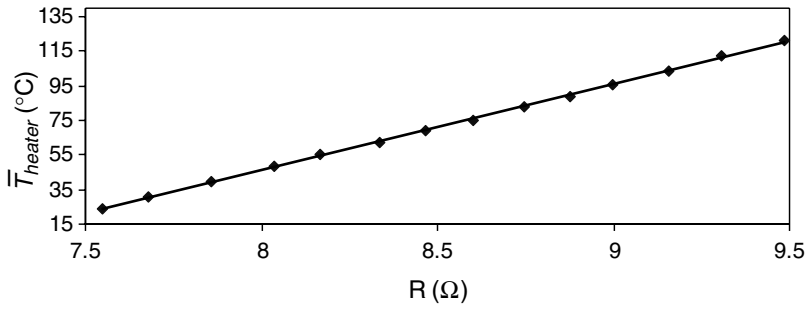

Fig. 4. Heater electrical resistance–temperature calibration curve.

the heat transfer coefficients, and the Nusselt numbers. The pressure data from the inlet and outlet was used to obtain the dimensionless cavitation index through the following expression:

$$\sigma = \frac{p_e - p_v}{\frac{1}{2}\rho u^2} \tag{1}$$

The electrical input power and heater resistance, respectively, were determined with

$$P = V \times I \tag{2}$$

and

$$R = V/I \tag{3}$$

The surface temperature at the base of the microchannels was then calculated as

$$\overline{T} = \overline{T}_{\text{heater}} - \frac{(P - \dot{Q}_{\text{loss}})t_s}{k_s A_p} \tag{4}$$

4.3.1. Non-boiling fluid flow

The exit fluid temperature was calculated with a calorimetric balance, and the average fluid temperature is expressed as

$$\overline{T}_F = \frac{T_i + T_e}{2} \tag{5}$$

Assuming that the walls of the channels behaved as one-dimensional fins with adiabatic tip, the power input was related to the average single-phase heat transfer coefficient in the channel

$$P - \dot{Q}_{\text{loss}} = \eta_o A_t \bar{h}_{sp}(\overline{T} - \overline{T}_F) \tag{6}$$

where η_o is the overall surface efficiency of the microchannel configuration:

$$\eta_o = \frac{N\eta_f A_f + (A_t - NA_f)}{A_t} \tag{7}$$

where

$$\eta_f = \frac{\tanh(mH)}{mH}, \quad m = \sqrt{\frac{\bar{h}_{sp}2(L+W)}{k_s WL}}, \quad A_f = 2W_b L \tag{8}$$

Eqs. (4)–(8) were employed to evaluate $\bar{h}_{sp}$ with an iterative scheme.

4.3.2. Boiling flow

During boiling flow the channel was sub-divided into two separate regions, a two phase region where boiling was occurring (L_{tp}) and a region where the flow was still single phase (L_{sp}). The length of each region was found through flow visualization for the non-cavitating flow. For the cavitating flow the channel was assumed to be entirely two phase (L_{tp}). The assumption of modeling the channel walls as a one-dimensional fin was carried over from the single phase analysis and used to calculate the average boiling heat transfer coefficient $\bar{h}_{tp}$ as follows:

$$\bar{h}_{tp}(\overline{T}_{tp} - T_{sat})(WL + A_f\eta_f) = \frac{(P - \dot{Q}_{\text{loss}})(W + W_b)L}{A_p} \tag{9}$$

The inlet and exit surface temperatures are given as

$$T_{si,sp} = T_i + \frac{(P - \dot{Q}_{\text{loss}})}{\overline{h_{sp}}A_s} \tag{10}$$

$$T_{se,sp} = T_{sat} + \frac{(P - \dot{Q}_{\text{loss}})}{\overline{h_{sp}}A_s} \tag{11}$$

Average wall temperature:

$$\overline{T}_{sp} = \frac{T_{si,sp} + T_{se,sp}}{2} \tag{12}$$

By calculating $\overline{T}_{sp}$, $\overline{T}_{tp}$ can be evaluated using a weighted average of the single phase and two phase wall temperature regions:

$$\overline{T}_{tp} = \frac{\overline{T}L - \overline{T}_{sp}L_{sp}}{L_{tp}} \tag{13}$$

The exit quality can be calculated using an energy balance where the net power supplied to the device and the mass flux are known

$$x_e = \frac{(P - \dot{Q}_{\text{loss}}) - \dot{m}c_p(T_{sat} - T_i)}{\dot{m}h_{fg}} \tag{14}$$

The uncertainties of the measured values, were obtained from the manufacturer's specification sheets, while the uncertainties of the derived parameters were calculated using the method developed by Kline and McClintock [78]. Uncertainties in the heat transfer coefficients, cavitation numbers, and average temperature are estimated to be 4.7%, 2.3%, and 1.2 °C respectively.

4.4. Heat losses

To minimize heat loss by conduction through the sides of the device, air gaps were etched into the silicon substrate along the length of the channels. In order to estimate the heat losses occurring in the intake and exit plenum, a one-dimensional fin analysis was performed. From this simple analysis it was found these heat losses were approximately 5–10% of the total power and could not be neglected (Fig. 5). To verify the estimated heat loss, electrical power was applied to an evacuated test section. During steady state conditions a temperature difference versus power curve was plotted and used to compare the heat loss associated with each experimental data point to the fin analysis. The results from this comparison showed very good agreement. The measured heat loss was then subtracted from the total heat supplied to the heat sink under forced flow conditions, and used for data analysis. Heat losses from the top and bottom surfaces were estimated by again assuming one-dimensional conduction. These results yielding minimal losses of ~0.03 W and ~0.015 W, respectively, compared to the 2–50 W applied at the heater, and these losses were neglected during data analysis.

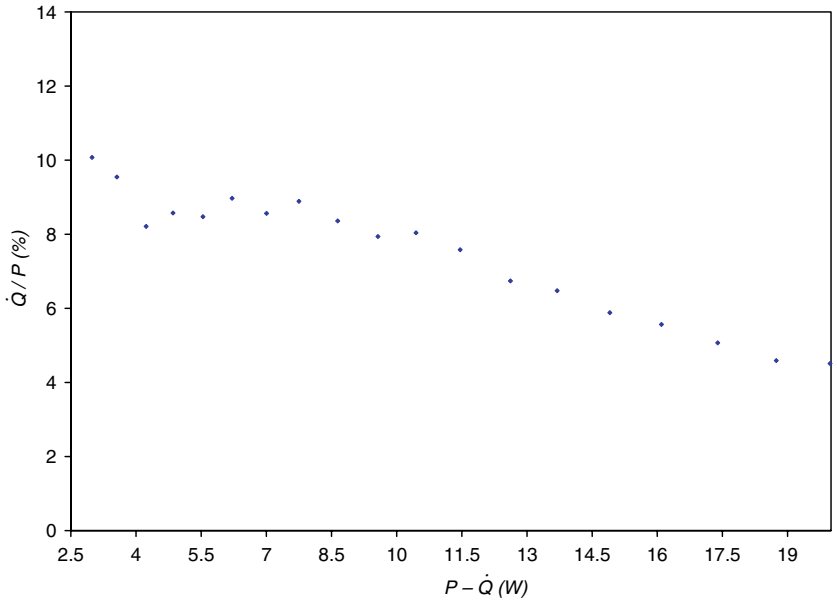

Fig. 5. Heat loss curve for cavitating conditions $G = 1368\ \mathrm{kg/m^2\,s}$.

5. Results and discussion

In the study of convection heat transfer, the flow field is frequently assumed to be independent of the thermal field, while the heat transfer is commonly understood as being strongly dependent on the hydrodynamic characteristics of the flow. Since the characteristics of the cavitating flow is primarily dictated by the hydrodynamic field it is useful to first study the phenomena without the presence of heat transfer, and then introduce thermal load to explore its effects on the flow field and vice versa. Concurring with this logic, adiabatic tests are initially reported (Section 5.1), followed by the heat transfer study (Section 5.2).

5.1. Hydrodynamics

For the adiabatic flow experiments, a fixed mass flux of 1368 kg/m^2 s was maintained at five different exit pressures. The exit pressure varied over a range corresponding to three different flow patterns: single phase flow (exit pressure of 480 kPa), transition to cavitating flow (exit pressure of 293 kPa), and cavitating flow pattern (288 kPa, 230 kPa, and 146 kPa).

The cavitation inception number obtained in the current study with R-123 is significantly higher than the reported values for water in short micro-orifices entrenched inside microchannels obtained by Mishra and Peles [41,45]. The increased cavitation susceptibility of the coolant compared to water can be attributed to the distinct difference in the physical properties of the two liquids and to higher dissolved air concentration. It is well documented and understood that water, having high surface tension ($\sigma = 0.07232$ N/m at 23 °C), can withstand significant tensile stress [11,79]. Since R-123 has low surface tension ($\sigma = 0.01545$ N/m at 23 °C) it is more prone to rupture at much higher pressures than water. However, low surface tension liquids, such as R-123, tend also to highly wet many engineering surfaces such as native oxide silicon surfaces. Such liquids flood surface nuclei and cause the effective nuclei radii to diminish. Thus, contrary to the affects of surface tension, the wettability of R-123 suppresses the activation of surface nuclei bubbles to promote cavitation. This suggests that unlike the results of Mishra and Peles for water flow over short micro-orifice, stream nuclei rather than surface nuclei are accountable for the initial appearance of inchoate bubbles in the current study. The dwell time necessary for stream nuclei to grow under low pressure ambient can be expressed as [1]

$$t = R_o \int_1^{R_f/R_o} \left[\frac{2(P_V - P_\infty)(1 - x^{-3})}{3\rho} + \frac{2P_{G0}(x^{-3k} - x^{-3})}{3(1-k)\rho} - \frac{2S(1-x^{-2})}{\rho R_o x} \right]^{-0.5} dx \tag{15}$$

Assuming a spherical stream nuclei of diameter 1 μm enter the orifice, the time required for the bubble to reach 10 μm under the saturation dissolved air concentration at the inlet conditions is estimated to be 0.246 μs. The time spent by the nuclei in the orifice is 21.5 μs for $G = 1368\ \mathrm{kg/m^2\,s}$. It follows that for the present flow conditions a stream nuclei has sufficient time to applicably grow and trigger cavitation.

Once cavitation is triggered in the microchannel, further pressure reduction succeeds in promoting very rapid extension of cavitation events downstream. The transition from cavitation inception to supercavitation which stretches downstream of the micro-orifice until the channel exit (270 micro orifice hydraulic diameters downstream) was

abrupt and partial cavitation was merely present over a very short range of cavitation numbers. Similar trend for water flow was observed by Mishra and Peles [41,45] for microchannels, and by Pennathur et al. [80] for cavitating flow over micro-hydrofoil. In conventional scale orifices the transition between cavitation inception to supercavitation occurred over a significantly broader range of cavitation numbers [24,30]. This supports the hypothesis made by Mishra and Peles [41,42,45] based on their results and the study of Pennathur et al. [80] that suggests that the transition from single-phase liquid flow to cavitating flow in microsystems is a condition which marks a major transformation between completely different hydrodynamic flow fields.

In the fully developed cavitation flow, various flow morphologies were present in the microchannel depending on the cavitation number and longitudinal location along the channel. Theses flow patterns are classified into five categories, which are schematically depicted in Fig. 6. They are

1. liquid single-phase,
2. liquid jet,
3. transition region,
4. annular and wavy-annular,
5. bubbly.

The flow patterns are mapped as a function of the cavitation number and longitudinal location in the channel and are shown in Fig. 7.

A thin liquid jet is observed for the cavitating flows at the orifice exit which extends up to 20 or 25 micro orifice hydraulic diameters downstream depending on the cavitation number (Fig. 8a). Alongside the main jet a thin liquid layer around the twin cavities is formed on the channel sidewalls. Further downstream a transition region is formed (Fig. 8b). It is apparent that the start point and length of this transition region is controlled by the cavitation number. For decreasing cavitation numbers the first appearance of the transition region occurs further downstream of the orifice and travels for an extended distance downstream. The wavy annular flow pattern is only observed for cavitation numbers less than about three and follows the same general trend of the two patterns described above, increasing in length as the cavitation index decreases (Fig. 8c). Following the transition region the vapor breaks into small bubbles and the bubbly flow pattern prevails (Fig. 8d). The bubbly flow pattern extends to the channel exit (Fig. 8e) and is the dominant flow condition for all the current experiments. It is significantly more dominant than for water flow in similar configuration

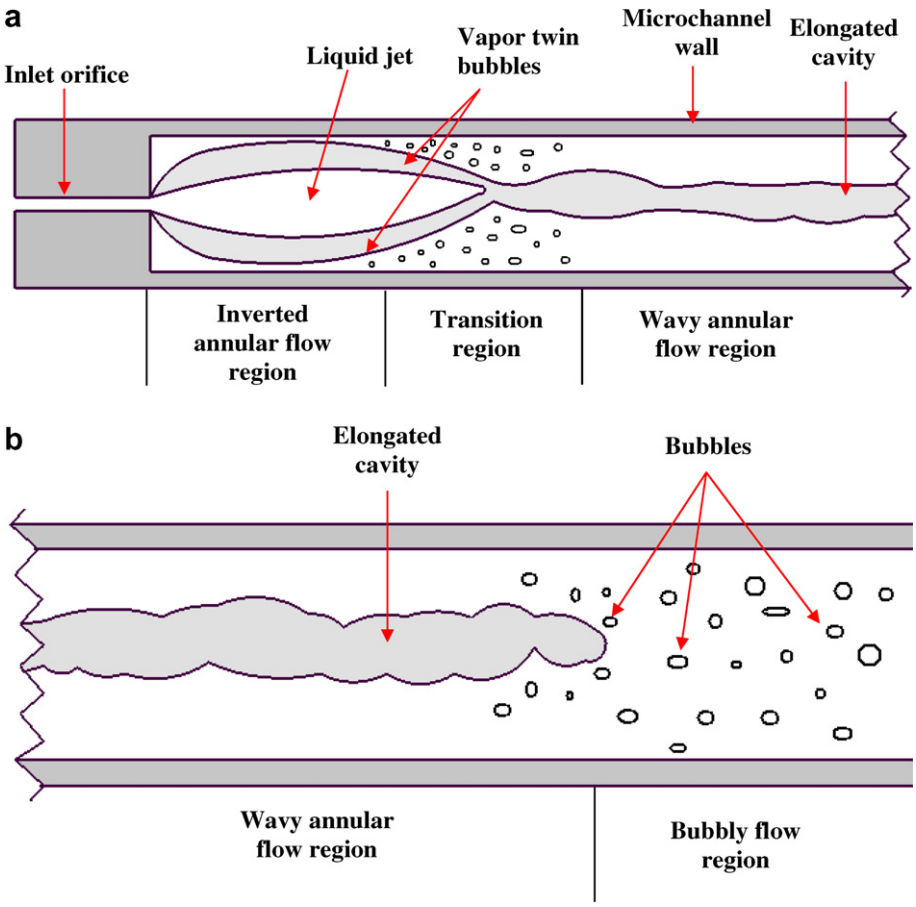

Fig. 6. Schematic of flow patterns: (a) microchannel inlet and (b) collapse of elongated bubble.

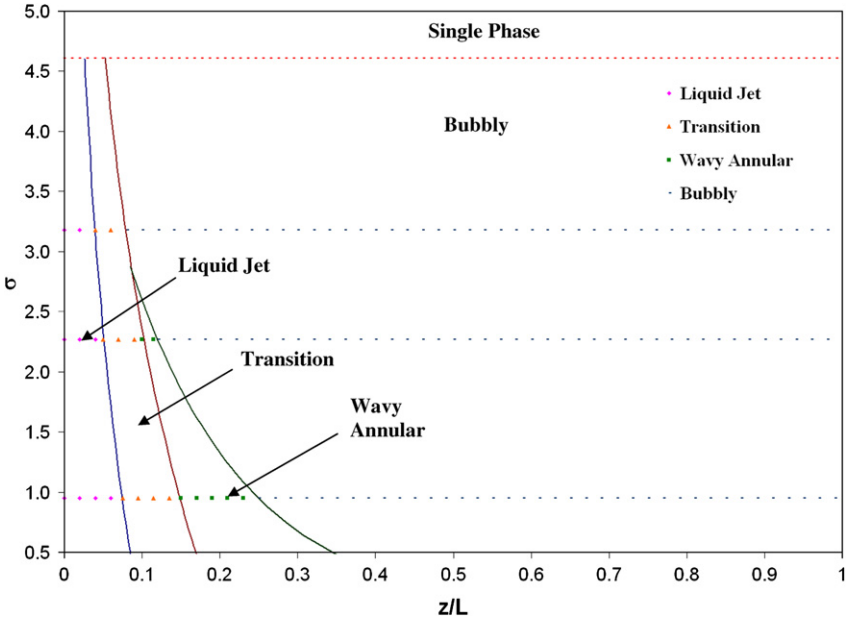

Fig. 7. Flow map under adiabatic conditions $G = 1368$ kg/m^2 s.

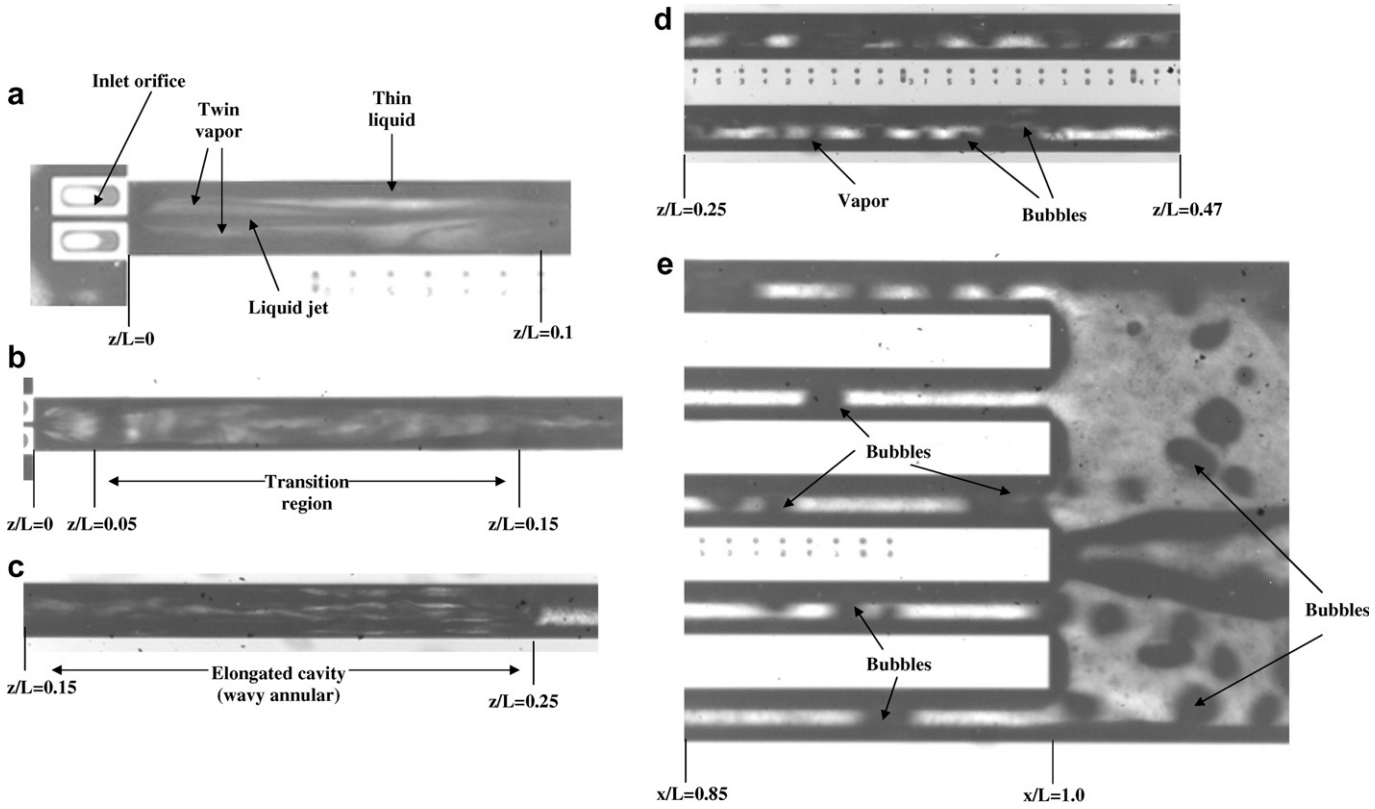

Fig. 8. (a) Liquid jet at inlet region single channel, adiabatic $G = 1368$ kg/m^2 s ($\sigma = 0.95$), (b) short cavity at the inlet region followed by a longer transition region adiabatic, $G = 1368$ kg/m^2 s ($\sigma = 2.27$), (c) wavy annular flow condition adiabatic, $G = 1368$ kg/m^2 s ($\sigma = 0.95$), (d) elongated bubbles middle of channel at adiabatic, condition $G = 1368$ kg/m^2 s ($\sigma = 3.18$) and (e) bubbly flow at the exit region for short cavities at adiabatic condition $G = 1368$ kg/m^2 s ($\sigma = 0.95$).

[42]. This is not entirely unexpected since R-123 has very low surface tension and has comparable viscosity to water. It has been reported in numerous archival reports [81] that viscous forces tend to abet the breakup of the vapor/gas interface while surface tension tends to prevent vapor break up. This is apparent in the current study.

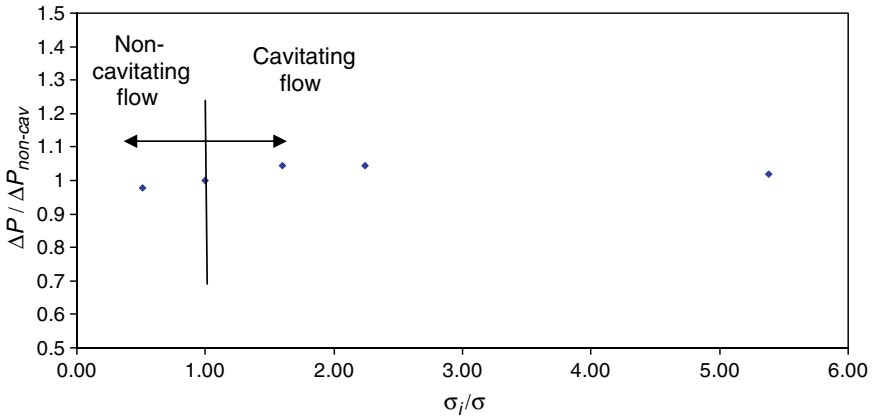

Fig. 9. Dimensionless pressure drop as a function of cavitation index $G = 1368\ \mathrm{kg/m^2\,s}$.

Fig. 9 displays the pressure drop between the inlet and exit plenum normalized by the pressure drop for non-cavitating flow as a function of a non-dimensionalized cavitation inception index. Similar to Mishra and Peles [42] the pressure loss required to promote cavitation is minimal compared to the non-cavitating conditions. It can therefore be concluded that the promotion and growth of cavitating flow patterns require only minor pressure drop penalties, at least under the current conditions studied in the current investigation.

5.2. Heat transfer

This section is divided into three subsections. The first subsection reports and discusses results obtained for single-phase liquid flow. The second subsection deals with cavitating flows with exit qualities lower than zero (termed non-boiling). The third subsection considers data pertaining to saturated boiling conditions (exit qualities larger than zero).

5.2.1. Single-phase liquid heat transfer

Fig. 10 depicts the experimental Nusselt number for the single-phase liquid flow and the corresponding value obtained using the following Shah and London [82] correlation for developing flow:

$$\overline{Nu} = 0.775(f \cdot Re)^{1/3}(x^*)^{-1/3} \tag{16}$$

$$\text{where} \quad x^* = x/(D_h \cdot Re \cdot Pr) \tag{17}$$

In order to account for the adiabatic top wall a correction factor, $F_{3,4}$ frequently used in various studies [65,83,84] was employed. This correction factor is the ratio of fully developed laminar Nusselt numbers Nu_3, and Nu_4 for three and four walls respectively

$$F_{3,4} = Nu_3/Nu_4 \tag{18}$$

where

$$Nu_3 = 8.235(1 - 1.883\beta + 3.767\beta^2 - 5.814\beta^3 + 5.361\beta^4 - 2.0\beta^5) \tag{19}$$

$$Nu_4 = 8.235(1 - 2.042\beta + 3.085\beta^2 - 2.477\beta^3 + 1.058\beta^4 - 0.186\beta^5) \tag{20}$$

The agreement between the correlation and the data for low Reynolds numbers is reasonable, while for the highest Reynolds number the correlation significantly underpredicts the result. It is also apparent that all the experimental data are larger than the correlation prediction. The discrepancy can be attributed to several factors. Shah and London's [82] correlation assumes uniform velocity at the inlet whereas in the current study the velocity profile is completely transformed by the presence of the jet emanating from the inlet orifice. In the immediate region downstream of the orifice the flow is detached and reattaches with the channel walls further downstream. This tends to extend the developing region. Furthermore, in flow through orifices there are three flow regimes [85]. In the first flow regime, the approach flow to the orifice is laminar and stays laminar even after passing via the orifice (laminar–laminar–laminar flow regime). Upon increasing the Reynolds number a second flow regime is encountered, wherein the laminar approach flow becomes turbulent immediately downstream of the orifice but relaminarizes upon traveling further downstream in the microchannel (laminar–turbulent–relaminarization). Finally, when the Reynolds number exceeds a critical value the approach flow becomes turbulent and remains turbulent at all locations downstream, leading to turbulent–turbulent–turbulent regime. At the conventional scale, Lakshmana Rao et al. [85] and Johansen [86,87] report a critical Reynolds number for the first appearance of turbulent flow immediately downstream of the orifice (laminar–turbulent–relaminarization regime) of $300 \leqslant Re_{\mathrm{Crit}} \leqslant 400$ for sharp-edged and quadrant-edged orifices ($0.2 \leqslant \beta \leqslant 0.6$). It has been confirmed [88] that the characteristics transition Reynolds number to laminar–turbulent–relaminarization at the

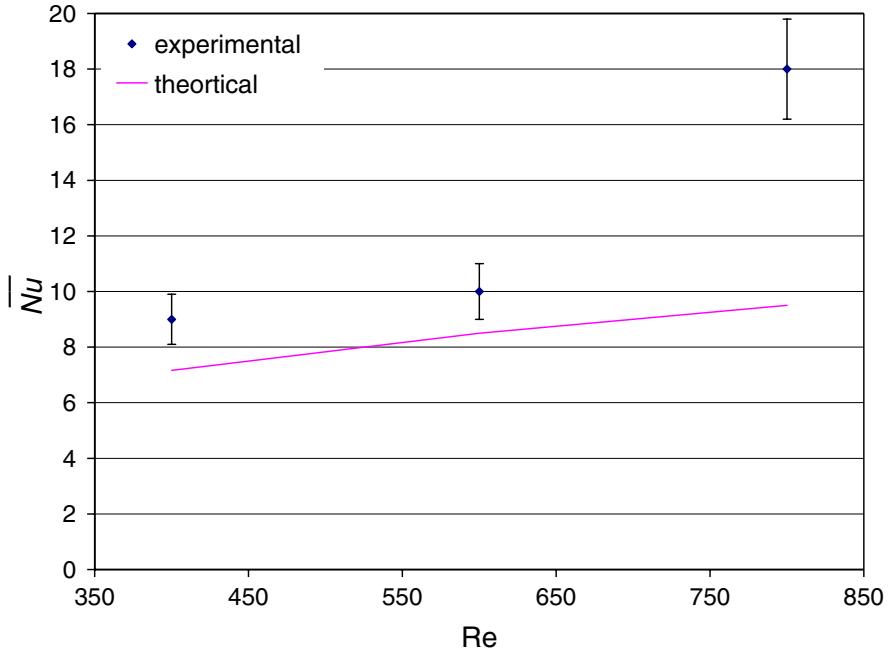

Fig. 10. Nusselt number comparison.

micro scale generally concur with conventional scale values. More recent studies on the dynamics of low Reynolds number flows in a symmetric channel with a sudden expansion [89–91] have revealed the existence of bifurcation points at a critical Reynolds number at which asymmetric flow states emerge. It was also found that the transition depends on the geometry under investigation. Alleborn et al. [91] extended the steady-state bifurcation diagrams to higher values of Re and found higher-order bifurcation points. It has been shown that the existence of these bifurcation points can significantly increase the heat transfer coefficient [92,93] which might explain the increase in the Nusselt number for the highest Reynolds number in the current study. It should be noted that Nusselt number correlations that capture the current configuration and account for bifurcation states (and early transition to turbulent flow) are not generally available; therefore, the Shah and London correlation should be merely considered as a reference.

5.2.2. Non-boiling flow

The average heat flux as a function of average surface temperature for non-cavitating and cavitating flow patterns at three mass velocities: 1368, 1036, and 622 kg/m^2 s are shown in Fig. 11. Table 1 provides the corresponding cavitation index for each mass velocity. A substantial reduction in the average surface temperature is obtained by promoting cavitating flows. The heat transfer enhancement during cavitating flows compared to non-cavitating flows is attributed to two distinct factors and can be better understood when expressing the surface temperature using Newton's law of cooling

$$T_s = \frac{q''}{hA} + T_m \tag{21}$$

A reduction of the surface temperature (for a given heat flux) can be brought about by increasing the heat transfer coefficient and/or reducing the flow temperature (the heat transfer area is unchanged during the study). The bubbly flow is characterized by exceedingly agitated flow (rapid mixing and advection), which results in elevated heat transfer coefficients. Furthermore, the presence of bubbles (gases or vaporous) in the flow effectively reduces the hydraulic diameter of the liquid phase and thus reduces the boundary layer thickness. It is well documented [94] that with diminishing length scale the heat transfer coefficient (h) increases in channel flows ($h \propto 1/D_h$). Similar reasoning has been used by several authors (e.g., [95]) to support the apparent heat transfer augmentation of annular flow compared to single-phase liquid flow in conventional systems.

Since it is postulated that gaseous rather than vaporous cavitation predominates the two-phase flow as evident by the high cavitation numbers at cavitation inception, liquid/vapor phase change is not predicted to ensue and affect the heat transfer (at least at low heat fluxes). As a result the two-phase mixture does not maintain constant temperature along the channel (as would be expected during boiling flow), and the reduction of the surface temperature during cavitating flow is not a result of lower flow temperature (at least at low heat fluxes) compared to the non-cavitating flows at the same mass velocities and heat fluxes.

The average non-boiling heat transfer coefficients for three different flow rates during cavitating flows are shown

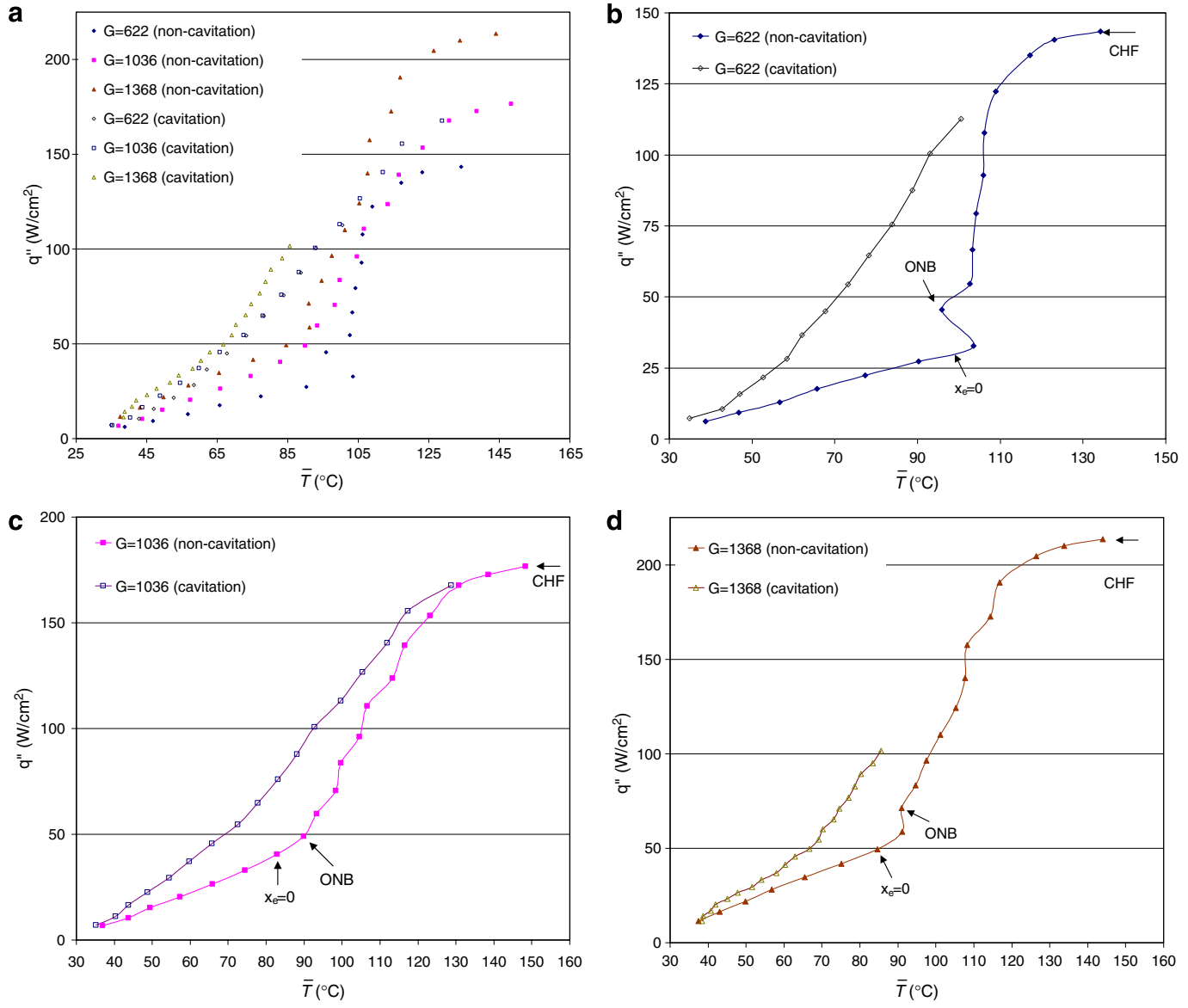

Fig. 11. Heat flux versus average surface temperature (a) all mass fluxes tested, (b) $G = 622$ kg/m^2 s, (c) $G = 1036$ kg/m^2 s and (d) 1368 kg/m^2 s.

Table 1
Adiabatic cavitation number for the tested flow rates

	G (kg/m^2 s)	σ_a
Cavitation	622	3.6
	1036	2.7
	1368	3.9
Non-cavitation	622	13.6
	1036	11.8
	1368	9.1

together with the results for the single-phase flows corresponding to low heat fluxes in Fig. 12. The average heat transfer coefficients of the cavitating flows compared to the single-phase flows is enhanced by 40%, 63%, and 84% for mass velocities of 622 kg/m^2 s, 1024 kg/m^2 s, and 1368 kg/m^2 s, respectively. It is apparent that the heat transfer coefficients of the cavitating flows increase with heat flux. However, the flow morphology is not strongly affected by the presence of heat transfer. This has been also shown in Fig. 7 by the relatively minor changes of the flow patterns with decreasing cavitation numbers (as long as the cavitating flow is fully developed and extends to the channel exit). The increase in the heat transfer coefficient might therefore be due to the intensification of the cavitation events and not through the modification of the flow patterns. That is, the bubbly flow can still predominate in the entire channel, however, the bubble count and size (void fraction) might be significantly altered. Furthermore, although the exit quality is still below zero the reduced local pressure downstream of the orifice can, under some conditions, promote nucleate boiling at temperatures well below the exit liquid and surface saturation temperature. However, the current experimental capabilities lack the

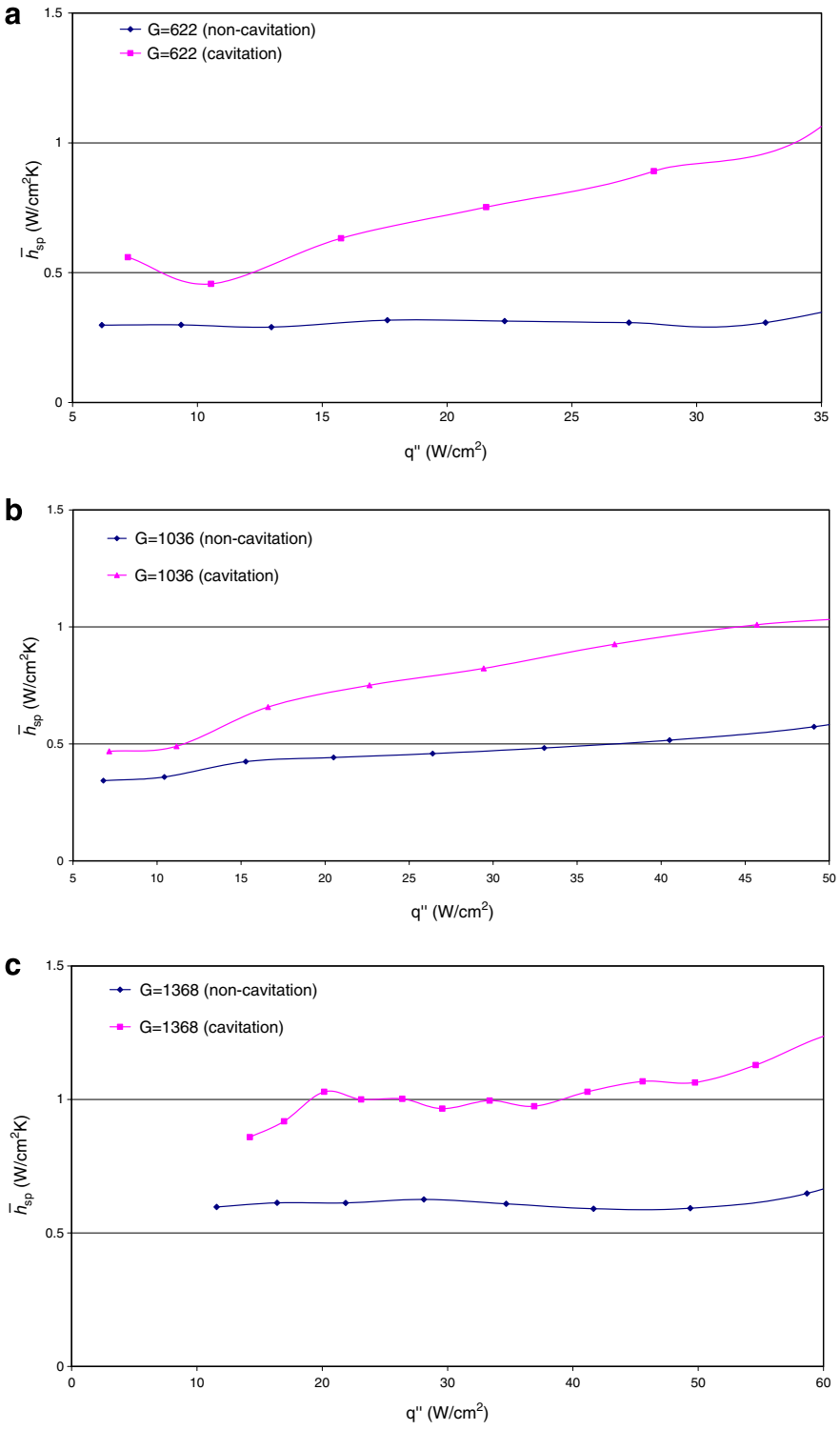

Fig. 12. Average single-phase heat transfer coefficient as a function of the average heat flux: (a) $G = 622\ \mathrm{kg/m^2\,s}$, (b) $G = 1036\ \mathrm{kg/m^2\,s}$ and (c) $G = 1368\ \mathrm{kg/m^2\,s}$.

ability to obtain local pressure measurements in order to fully account and quantify the relationship between cavitating flow morphologies and the heat transfer coefficient.

5.2.3. Boiling flow

From Fig. 11 it is apparent that the characteristic heat flux - surface temperature trend of the cavitating flow is less affected by the presence of boiling than the non-cavitating flow. For the non-cavitating flow the abrupt modification of the slope marks a rapid change from boiling inception to fully developed nucleate boiling. This is also linked with the significant temperature overshooting frequently observed in this study and also shown in Fig. 11b and d. With no temperature overshooting (Fig. 11c) the transition

from boiling inception to fully developed nucleate boiling is accompanied through a 'partial boiling' zone. Since the cavitating flow is a two-phase phenomenon regardless of the heat flux the transition to boiling flow is not marked by a distinct condition and therefore temperature hysteresis (overshooting) is not a characteristic of cavitating-boiling flows.

Conventional scale knowledge tends to classify the heat transfer mechanisms into two categories (in the pre critical heat flux conditions): convective boiling and nucleate

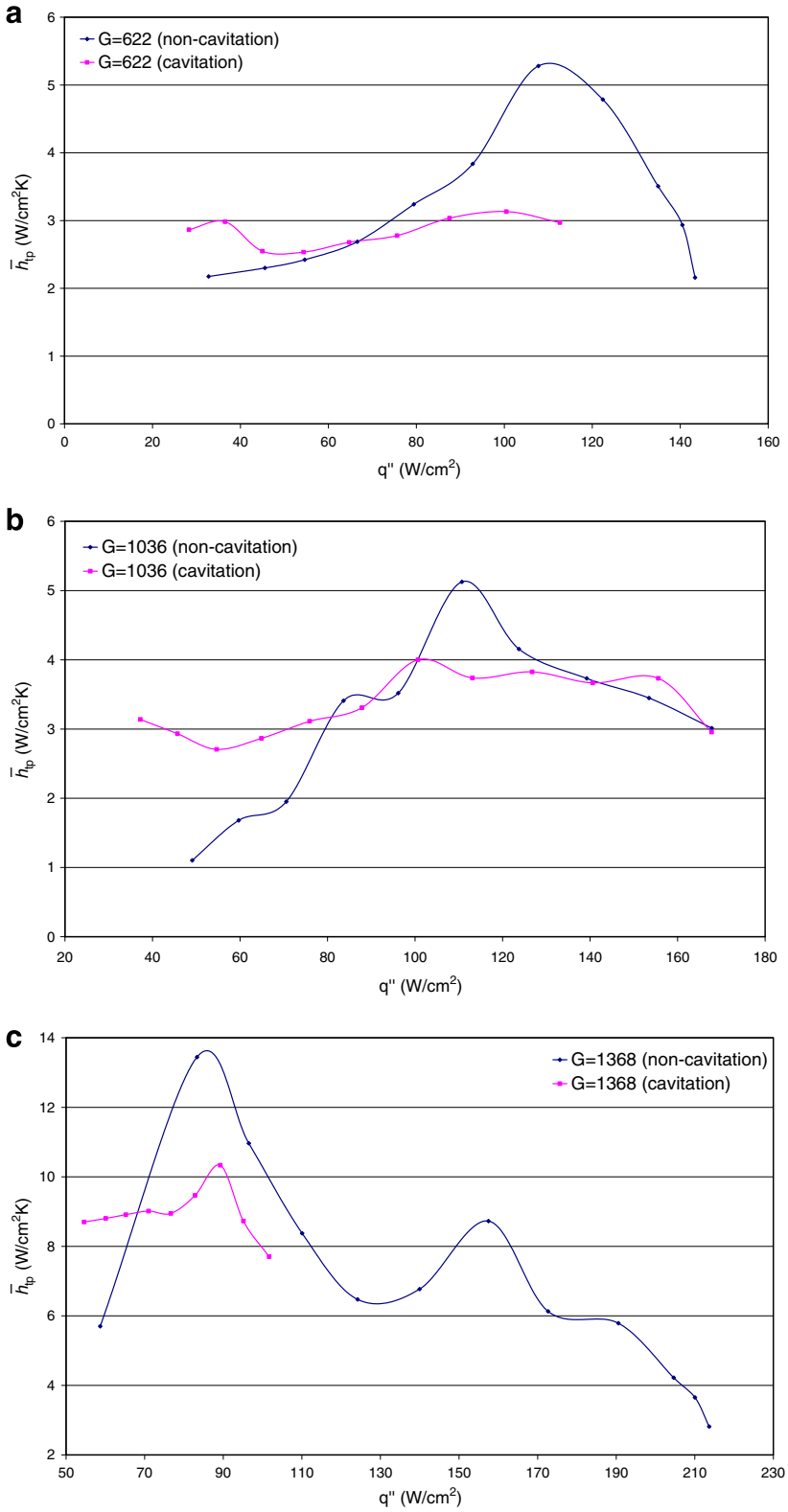

Fig. 13. Boiling heat transfer coefficient for cavitating and non-cavitating flow: (a) $G = 622$ kg/m^2 s, (b) $G = 1036$ kg/m^2 s, and (c) $G = 1368$ kg/m^2 s.

boiling. Convective boiling is characterized by the dependency of the heat transfer coefficient on mass velocity and exit quality, while nucleate boiling is dependent on heat flux and weakly dependent on exit quality and mass velocity. In the last several years relatively large numbers of studies have been dedicated to unveil the heat transfer mechanism prevailing during boiling flow in microchannels [47,55,58, 59,62,63,71], and a definite conclusion is far from being settled. The disagreement in the heat transfer community is well documented in several recent excellent reports [47, 63,71]. Thome and co-workers approach [47,63] is definitely refreshing and might be the proper avenue to pursue for microchannels boiling flows. However, the utilization of a new approach requires sufficient evidence (experimental validation) to justify its use. Therefore, in the current study we adopt a conservative approach based on conventional scale classifications to identify the heat transfer mechanisms. As shown in Fig. 13 the average two-phase heat transfer coefficient (corresponding to moderate to high heat fluxes) of the cavitating flows varies little with heat flux even at high heat fluxes and increases considerably with mass velocity. This suggests that the predominant heat transfer mechanism is convective boiling for all mass velocities and is dictated by the cavitating hydrodynamic flow field. The large increase in the heat transfer coefficient between the data for $G = 1036\ \mathrm{kg/m^2\,s}$ and $G = 1368\ \mathrm{kg/m^2\,s}$ can also imply that the flow field for the high mass velocity flow is turbulent. The heat transfer coefficient of the non-cavitating flows is strongly affected by the thermal field. At low heat fluxes the heat transfer coefficient increases with heat flux, then reaches a maximum before decreasing. While the increasing trend of h_{tp} with heat flux for low and moderate mass velocities ($G = 622\ \mathrm{kg/m^2\,s}$ and $G = 1036\ \mathrm{kg/m^2\,s}$) stretches over relatively large range of heat fluxes, the data for the high mass velocity peaks at a very low heat flux (also quality), and thereafter monotonically decreases. This suggests that for high mass velocities the heat transfer is dominated by convective boiling while at medium and low mass velocities the heat transfer is dominated by nucleate boiling. If one assumes nucleate boiling to dominate the heat transfer the heat transfer coefficient should be independent of mass velocity and exit quality. If the data for the high mass velocity is eliminated the heat transfer coefficient seems to vary little with mass velocity, suggesting nucleate boiling heat transfer. The bubble nucleation emanating from the surface and the bubble flow detected during boiling in the low and moderate mass velocity of the non-cavitating flow do in fact support the predomination of nucleate boiling.

6. Conclusions

Convective heat transfer of R-123 in the presence of assorted cavitating flow patterns has been investigated and discussed in flow through rectangular micro-orifices entrenched inside micro channels. The main conclusions drawn from this study are:

1. Bubbly flow morphology dominates fully developed cavitating flow of low surface tension liquids like R-123 in microchannels.
2. Significant heat transfer enhancement was obtained with cavitating single-phase flows compared to non-cavitating single-phase flows.
3. When boiling was initiated the deviation between the cavitating and non-cavitating flows diminishes with heat flux.
4. The effect of boiling on the heat transfer characteristics was less detrimental for cavitating flows compared to non-cavitating boiling flows. Furthermore, for non-cavitating flows the onset of nucleate boiling was accompanied by temperature overshooting. This did not occur for cavitating flow.
5. It appears that the heat transfer mechanism of the cavitating flows when boiling is triggered is dominated by convective boiling, while for the non-cavitating flows at low to medium qualities the heat transfer mechanism appears to be nucleate boiling and at higher qualities to be convective boiling.

References

[1] C.E. Brennen, Cavitation and Bubble Dynamic, Oxford University Press, Oxford, UK, 1995.
[2] H.-Y. Kim, Y.G. Kim, B.H. Kang, Enhancement of natural convection and pool boiling heat transfer via ultrasonic vibration, Int. J. Heat Mass Transfer 47 (2004) 2831–2840.
[3] R.M. Fand, The influence of acoustic vibrations on heat transfer by natural convection from a horizontal cylinder to water, J. Heat Transfer 8 (1965) 309–310.
[4] K.W. Li, J.D. Parker, Acoustical effects on free convective heat transfer from a horizontal wire, J. Heat Transfer 89 (1967) 277–278.
[5] S.W. Wong, W.Y. Chon, Effects of ultrasonic vibration on heat transfer to liquids by natural convection and boiling, AIChE J. 15 (1969) 281–288.
[6] Y. Iida, K. Tsutsui, Effects of ultrasonic waves on natural convection, nucleate boiling and film boiling heat transfer from a wire to a saturated liquid, Exp. Therm. Fluid Sci. 5 (1992) 108–115.
[7] D.W. Zhou, D.Y. Liu, X.G. Hu, C.F. Ma, Effect of acoustic cavitation on boiling heat transfer, Exp. Therm. Fluid Sci. 26 (2002) 931–938.
[8] A.E. Bergles, P.H. Newell Jr., The influence of ultrasonic vibrations on heat transfer to water flowing in annuli, Int. J. Heat Mass Transfer 8 (1965) 1273–1280.
[9] A.E. Bergles, The influence of flow vibrations on forced-convection heat transfer, J. Heat Transfer 7 (1964) 559–560.
[10] R.E.A. Arndt, Cavitation in fluid machinery and hydraulic structures, Annu. Rev. Fluid Mech. 13 (1981) 273–328.
[11] R.T. Knapp, J.W. Daily, F.G. Hammit, Cavitation, McGraw-Hill, New York, 1970.
[12] M.S. Plesset, The dynamic of cavitation bubbles, J. Appl. Mech. 16 (1949) 277–282.
[13] L. Rayleigh, On the pressure developed in liquid during the collapse of spherical cavity, Philos. Mag. 34 (1917) 94–98.
[14] F.R. Young, Cavitation, McGraw-Hill, New York, 1989.
[15] D.D. Joseph, Cavitation and the state of stress in a flowing liquid, J. Fluid Mech. 366 (1998) 367–378.
[16] B. Ran, B.J. Katz, The response of microscopic bubbles to sudden change in ambient pressure, J. Fluid Mech. 244 (1991) 91–115.
[17] M. Kjeldsen, R.E.A. Arndt, M. Effertz, Spectral characteristics of sheet/cloud cavitation, J. Fluids Eng. 122 (2000) 481–487.

[18] R. Young, Cavitation in pumps, pipes, and valves, Process Eng. 71 (1990) 47–49.
[19] J.P. Tullis, Choking and supercavitating valves, J. Hydraul. Div. 97 (1971) 1931–1945.
[20] T.S. Koivula, A.U. Ellman, Cavitation behavior of hydraulic orifices and valves, SAE Trans. 107 (1998) 387.
[21] Z. Bikai, H. Yan, T. Zhang, L. Zhuangyun, Experimental investigation of the flow characteristics of small orifices and valves in water hydraulics, J. Process Mech. Eng. 216 (4) (2002) 235–245.
[22] J.P. Tullis, Hydraulics of Pipelines, John Wiley & Sons Inc., New York, USA, 1989.
[23] P.R. Gogate, I.Z. Shirgaonkar, M. Sivakumar, P. Senthilkumar, N.P. Vichare, A.B. Pandit, Cavitation reactors: efficiency assessment using a model reaction, AIChE J. 47 (11) (2001) 2526–2538.
[24] Y. Yan, R.B. Thorpe, Flow regime transitions due to cavitation in the flow through an orifice, Int. J. Multiphase Flow 16 (6) (1990) 1023–1045.
[25] J.P. Tullis, R. Govindarajan, Cavitation and size scale effect for orifices, J. Hydraul. Div. 99 (1973) 417–430.
[26] F. Numachi, M. Yamabe, R. Oba, Cavitation effect on the discharge coefficient of the sharp-edge orifice plate, J. Basic Eng. 82 (1) (1960) 1–11.
[27] K. Ramamurthi, K. Nandakumar, Characteristics of flow through small sharp-edged cylindrical orifices, Flow Meas. Instrum. 10 (3) (1999) 133–143.
[28] K. Ramamurthi, S.R. Patnaik, Influence of periodic disturbances on inception of cavitation in sharp-edged orifices, Exp. Fluids 33 (5) (2002) 720–727.
[29] N.H. Nurick, Orifice cavitation and its effect on spray mixing, J. Fluids Eng. 98 (4) (1976) 681–687.
[30] J.W. Ball, J.P. Tullis, Predicting cavitation in sudden enlargements, J. Hydraul. Div. 101 (7) (1975) 857–870.
[31] M.J. Robinson, F.G. Hammitt, Detailed damage characteristics in cavitating venturi, J. Basic Eng. 89 (1967) 511–517.
[32] R.D. Ivany, F.G. Hammitt, T.M. Mitchell, Cavitation bubble collapse observations in venturi, J. Basic Eng. 88 (1966) 649–655.
[33] K. Berman, T.C. Carnavos, Some experiments with two-dimensional cavitating venturis, Jet Propulsion 27 (1957) 148–150.
[34] D. Chatterjee, V.H. Arakeri, Some investigations on the use of ultrasonics in travelling bubble cavitation control, J. Fluid Mech. 504 (2004) 365–389.
[35] Y. Ito, R. Oba, Cavitation shock pressures in a venturi, No. 306, Reports of the Institute of High Speed Mechanics, Tohoku University, vol. 37, 1978, pp. 29–42.
[36] J.H. Gummer, M.T. Thew, Venturi investigations into cavitation in ethylene glycol/water mixtures, J. Process Mech. Eng. 212 (1998) 235–250.
[37] C. Xu, S.D. Heister, R. Field, Modeling cavitating venturi flows, J. Propul. Power 18 (2002) 1227–1234.
[38] I.Y. Chen, S.G. Liou, J.S. Sheu, Small cavitating venturi performance characteristics at low inlet subcooling, J. Thermophys. Heat Transfer 12 (1998) 602–605.
[39] K. Sato, K. Hachine, Y. Saito, Inception and dynamics of traveling-bubble-type cavitation in a venturi, in: Proc. ASME/JSME Joint Fluids Eng./4th ASME/JSME Joint Fluids Eng. Conf. 2A, Honolulu, HI, United States, 2003, pp. 279–285.
[40] G.L. ine, Y.T. Shen, Bubble dynamics and cavitation inception in cavitation susceptibility meter, J. Fluids Eng. 108 (4) (1986) 444–452.
[41] C. Mishra, Y. Peles, Cavitation in flow through a micro-orifice inside a silicon microchannel, Phys. Fluids 17 (1) (2005) 013601-1–013601-15.
[42] C. Mishra, Y. Peles, Flow visualization of cavitating flows through a rectangular slot micro-orifice ingrained in a microchannel, Phys. Fluids 17 (11) (2005) 113602–113602-14.
[43] C. Mishra, Y. Peles, An experimental investigation of hydrodynamic cavitation in micro-venturis, Phys. Fluids 18 (2006).
[44] C. Mishra, Y. Peles, Development of cavitation in refrigerant (R-123) flow inside rudimentary microfluidic systems, J. Microelectromech. Syst. 15 (5) (2006) 1319–1329.
[45] C. Mishra, Y. Peles, Size scale effects on cavitating flows through micro-orifices entrenched in rectangular microchannels, J. Microelectromech. Syst. 14 (5) (2005) 987–999.
[46] B. Schneider, A. Koşar, C.-J. Kuo, C. Mishra, G.S. Cole, R.P. Scaringe, Y. Peles, Cavitation enhanced heat transfer in microchannels, J. Heat Transfer 128 (12) (2006) 1293–1304.
[47] J.R. Thome, Boiling in microchannels: a review of experiment and theory, Int. J. Heat Fluid Flow 25 (2004) 128–139.
[48] L. Zhang, E.N. Wang, K.E. Goodson, T.W. Kenny, Phase change phenomena in silicon microchannels, Int. J. Heat Mass Transfer 48 (8) (2005) 1572–1582.
[49] P. Balasubramanian, S.G. Kandlikar, Experimental study of flow patterns, pressure drop, and flow instabilities in parallel rectangular minichannels, Heat Transfer Eng. 26 (3) (2005) 20–27.
[50] M. Lee, Y.Y. Wong, M. Wong, Y. Zohar, Size and shape effects on two-phase flow patterns in microchannel forced convection boiling, J. Micromech. Microeng. 13 (1) (2003) 155–164.
[51] P. Cheng, H.Y. Wu, Visualization and measurements of periodic boiling in silicon microchannels, Int. J. Heat Mass Transfer 46 (14) (2003) 2603–2614.
[52] L. Jiang, M. Wong, Y. Zohar, Forced convection boiling in microchannel heat sink, J. Microelectromech. Syst. 10 (1) (2001) 80–87.
[53] L. Zhang, J. Koo, L. Jiang, M. Asheghi, K.E. Goodson, J.G. Santiago, Measurements and modeling of two-phase flow in microchannels with nearly constant heat flux boundary conditions, J. Microelectromech. Syst. 11 (1) (2002) 12–19.
[54] J. Li, G.P. Peterson, Boiling nucleation and two-phase flow patterns in forced liquid flow in microchannels, Int. J. Heat Mass Transfer 48 (23) (2005) 4797–4810.
[55] M.E. Steinke, S.G. Kandlikar, An experimental investigation of flow boiling characteristics of water in parallel microchannels, J. Heat Transfer 126 (4) (2004) 518–526.
[56] A. Koşar, C.-J. Kuo, Y. Peles, Reduced pressure boiling heat transfer in rectangular microchannels with interconnected reentrant cavities, J. Heat Transfer 127 (10) (2005) 1106–1114.
[57] R. Yun, Y. Kim, M.-S. Kim, Convective boiling heat transfer characteristics of CO_2 in microchannels, Int. J. Heat Mass Transfer 48 (2) (2005) 235–242.
[58] A. Koşar, C.-J. Kuo, Y. Peles, Boiling heat transfer in rectangular microchannels with reentrant cavities, Int. J. Heat Mass Transfer 48 (23–24) (2005) 4867–4886.
[59] W. Qu, I. Mudawar, Flow boiling heat transfer in two-phase microchannel heat sink? I. Experimental investigation and assessment of correlation methods, Int. J. Heat Mass Transfer 46 (15) (2003) 2755–2771.
[60] J. Xu, S. Shen, Y. Gan, Y. Li, W. Zhang, Q. Su, Transient flow pattern based microscale boiling heat transfer mechanisms, J. Micromech. Microeng. 15 (6) (2005) 1344–1361.
[61] S. Grohmann, Measurement and modeling of single-phase and flow-boiling heat transfer in microtubes, Int. J. Heat Mass Transfer 48 (19–20) (2005) 4073–4089.
[62] S.G. Kandlikar, Heat transfer mechanisms during flow boiling in microchannels, J. Heat Transfer 126 (1) (2004) 8–16.
[63] V. Dupont, J.R. Thome, Evaporation in microchannels: infuence of the channel diameter on heat transfer, Microfluid Nanofluid 1 (2) (2005) 119–127.
[64] M. Piasecka, M.E. Poniewski, Hysteresis phenomena at the onset of subcooled nucleate flow boiling in microchannels, Heat Transfer Eng. 25 (3) (2004) 44–51.
[65] W. Qu, I. Mudawar, Prediction and measurement of inception boiling heat flux in micro-channel heat sink, Int. J. Heat Mass Transfer 45 (19) (2002) 3933–3945.
[66] H.Y. Wu, P. Cheng, Boiling instability in parallel silicon microchannels at different heat flux, Int. J. Heat Mass Transfer 47 (2004) 3631–3641.
[67] R. Mosdorf, P. Cheng, H.Y. Wu, M. Shoji, Non-linear analyses of flow boiling in microchannels, Int. J. Heat Mass Transfer 48 (21–22) (2005) 4667–4683.

[68] A.E. Bergles, S.G. Kandlikar, On the nature of critical heat flux in microchannels, J. Heat Transfer 127 (2005) 101–107.
[69] A. Koşar, C.-J. Kuo, Y. Peles, Suppression of boiling flow oscillations in parallel microchannels with inlet restrictors, J. Heat Transfer 128 (3) (2006) 251–260.
[70] L. Jiang, M. Wong, Y. Zohar, Phase change in microchannel heat sinks with integrated temperature sensors, J. Microelectromech. Syst. 8 (4) (1999) 358–365.
[71] J. Lee, I. Mudawar, Two-phase flow in high-heat-flux micro-channel heat sink for refrigeration cooling applications: Part II – heat transfer characteristics, Int. J. Heat Mass Transfer 48 (5) (2005) 941–955.
[72] A. Koşar, Y. Peles, Thermal-hydraulic performance of MEMS-based pin fin heat sink, J. Heat Transfer 128 (2) (2006) 121–131.
[73] Y. Peles, A. Koşar, C. Mishra, C.-J. Kuo, B. Schneider, Forced convective heat transfer across a pin fin micro heat exchanger, Int. J. Heat Mass Transfer 48 (17) (2005) 3615–3627.
[74] A. Koşar, C. Mishra, Y. Peles, Laminar flow across a bank of low aspect ratio micro pin fins, J. Fluids Eng. 127 (3) (2005) 419–430.
[75] R.S. Prasher, J. Dirner, J.-Y. Chang, A. Myers, D. Chau, D. He, S. Prstic, Nusselt number and friction factor of staggered arrays of low aspect ratio micro pin fins under cross flow, J. Heat Transfer 129 (2007) 141–153.
[76] R.C. Murphy, A.E. Bergles, Subcooled flow boiling of fluorocarbons—hysteresis and dissolved gas effects on heat transfer, in: Proceedings of Heat Transfer and Fluid Mechanics Inst, Stanford University Press, 1972, pp. 400–416.
[77] M. Steinke, S.G. Kandlikar, Control and effect of dissolved air in water during flow boiling in microchannels, Int. J. Heat Mass Transfer 47 (2004) 1925–1935.
[78] S. Kline, F.A. McClintock, Describing uncertainties in single-sample experiments, Mech. Eng. 75 (1) (1953) 3–8.
[79] R.T. Knapp, Cavitation and nuclei, Trans. ASME 80 (1958) 1315–1324.
[80] S. Pennathur, Y. Peles, A.H. Epstein, Cavitation at micro-scale in MEMS fluid machinery, in: Proc. ASME Int. Mech. Eng. Congress and Expos., New Orleans, USA, 2002, pp. 87–94.
[81] A.H. Lefebvre, Atomization and Sprays, Hemisphere Pub. Corp., New York, 1989.
[82] R.K. Shah, A.L. London, Laminar flow forced convection in ducts, Advances in Heat Transfer, Suppl. 1, Academic Press, New York, 1978.
[83] R.J. Phillips, Advances in thermal modeling of electronic components, in: A. Bar-Cohen, A.D. Kraus (Eds.), Microchannel Heat Sink, vol. 2, 1990, pp. 109–184.
[84] S.F. Choquette, M. Faghri, M. Charmchi, Y. Asako, Optimum design of microchannel heat sink, in : Micro-electro-mechanical system (MEMS), DSC-vol. 59, 1996, pp. 115–126.
[85] N.S. Lakshmana Rao, K. Sridharan, S.H. Alvi, Critical Reynolds number for orifice and nozzle flows in pipes, J. Hydraul. Res. 15 (1977) 167–178.
[86] F.C. Johansen, The influence of pipe diameter on orifice discharge coefficients, Annu. Rev. Fluid Mech. 149 (1930) 679–681.
[87] F.C. Johansen, Flow through pipe orifices at low Reynolds numbers, Proc. Roy. Soc. London 126 (1930) 231–245.
[88] C. Mishra, Y. Peles, Incompressible and compressible flows through rectangular micro-orifices entrenched in silicon microchannels, J. Microelectromech. Syst. 14 (5) (2005) 1000–1012.
[89] T. Hawa, Z. Rusak, The dynamic of a laminar flow in a symmetric channel with a sudden expansion, J. Fluid Mech. 436 (2001) 283–320.
[90] F. Battaglia, S.J. Tavener, A.K. Kulkarni, C.L. Merkle, Bifurcation of low Reynolds Number flows in symmetric channel, AIAA J. 35 (1997) 99–105.
[91] N. Alleborn, K. Nandakumar, H. Raszillier, F. Durst, Further contributions on the two-dimensional flow in a sudden expansion, J. Fluid Mech. 330 (1997) 169–188.
[92] N. Seki, S. Fukusako, T. Hirata, Laminar heat transfer downstream of a sudden enlargement of a duct, Bull. JSME 21 (152) (1978) 254–257.
[93] T. Ota, H. Yanaoka, T. Hata, Numerical analysis of laminar flow and heat transfer in a two-dimensional symmetrically enlarged channel, Trans. Japanese Soc. Mech. Eng., Part B 60 (579) (1994) 3930–3936.
[94] F.P. Incropera, D.P. DeWitt, Introduction to Heat Transfer, fourth ed., Wiley, New York, 2002.
[95] J.G. Collier, J.R. Thome, Convective Boiling and Condensation, third ed., Oxford Science Publications, Oxford, 1994, pp. 255–259.